Measurement and Analysis of Flow of Concentrated Fiber Suspensions through a 2-D Sudden Expansion Using UVP

Julia Claesson and Anders Rasmuson
Dept. of Chemical and Biological Engineering, Chalmers University of Technology, SE-412 96 Gothenburg, Sweden

Johan Wiklund
SIK-The Swedish Institute for Food and Biotechnology, PO Box 5401, SE-402 29 Gothenburg, Sweden

Tomas Wikström
Metso Paper Sundsvall AB, SE-851 94 Sundsvall, Sweden

DOI 10.1002/aic.13881
Published online August 9, 2012 in Wiley Online Library (wileyonlinelibrary.com).

The ultrasound velocity profiling technique (UVP) was used to study flow structures after a two-dimensional (2-D) 1:11 sudden expansion of pulp fiber suspensions at varied average velocities (1–2.2 m/s) and concentrations (1.8 and 2.8 wt %). One advantage of studying jet geometry is the potential to investigate the main flow structures away from walls. Measurements done at the same percent of the total jet length, at constant concentration, show that an increase in flow rate gave a faster decrease in centerline velocity and a quicker increase in jet width. Increasing the concentration, at the same jet length, the centerline velocity was more stable and the width of the mixing layer increased more rapidly. Comparisons with CFD simulations in the laminar regime, using the Bingham plastic model, show that the main flow structures were captured if the yield stress used in the simulations is approximately 20% of the measured using a rheometer. *AIChE J,* 59: 1012–1021, 2013
Keywords: fibers, fluid mechanics, multiphase flow, suspensions

Introduction

A jet is a flow geometry that has a wide range of engineering applications, e.g., in mixing.[1–3] The flow characteristics of various kinds of single-phase Newtonian jets and boundary layers have been extensively studied by many research groups. Mathematical models describing the boundary layer flow and jets in Newtonian fluids have been derived.[4,5]

Jet flows with particle suspensions remain, in contrast, largely unexplored. This class of flow is strikingly different from single-phase flows as particle concentration inhomogeneities are generated through particle collisions, shear-induced particle migration, density differences between the particles and the carrier fluid, and, in the case of papermaking fibers, flocculation created by means of frictional forces between the particles. Non-Newtonian effects occur in pulp fiber suspension already at concentrations of approximately 1 wt %.[6,7] Several industrial process fluids exhibit non-Newtonian flow behavior depending on the local concentration of a solid, for example a fibrous constituent. Typical examples are found in the bio-process, food, and paper and pulp industries.[8] A common method to characterize momentum transfer in non-Newtonian fluids is to determine an effective viscosity by using the local shear rate as well as particle concentration.[9]

The dispersed phase influence on the flow structure and the turbulence level of solid–liquid and solid-gas jets has been studied by Fan et al., Sheen et al., and Virdung and Rasmuson.[10–12] These studies have investigated the spreading rate, differences in flow velocities between the phases as well as fluctuations in the fluid. It has been found that the spreading rate and the decrease in centerline velocity are smaller in a two-phase jet than in a single-phase jet.[10–11] In the study by Virdung and Rasmuson[12] it was found that the axial root mean square (RMS) velocities increase with an increase in concentration of solid particles (1.5 mm in dia.) and these were larger in the disperse phase.

A few studies of laminar non-Newtonian jets have been published. Jafri and Vradis[13] solved numerically the boundary layer equations for the evolution of the laminar jets of Herschel-Bulkley fluids. Their findings show that the evolution of the jet is identical to and independent of the dimensionless yield number ($Y = \tau_y D/\mu_{\text{ref}} U_0$), in the initial stages of jet development. The plug-zone present along the centerline dominates the flow evolution away from the inlet region. They also showed that for yield stress exhibiting fluids no similarity profiles ever develop in the far-field region of the flow-field. Stehr and Schneider[14] investigated non-Newtonian planar and asymmetric power law jet flows with a numerical finite element method at a low Reynolds number. From their simulations they concluded that the classical

Correspondence concerning this article should be addressed to A. Rasmuson at rasmuson@chalmers.se.

boundary layer theory was invalid for lower values of the power law index, $n < 2/3$, due to the change in the momentum flow in the jet.

In pulp and paper mills the flow through sudden expansions, e. g., in mixers, screens and in the headbox are important operations that influence the efficiency and the quality of the end product.[15] Another advantage of studying jet geometry is the potential to investigate the main flow structures without involving wall effects like dewatering.[4,13,16,17] The flow of pulp suspensions consists of water and fibers that flocculate and form coherent fiber networks already at a concentration of approximately 1 wt %. To compare fiber tendency to form a network in fiber suspensions with different fiber dimensions Kerekes et al.[18] defined a crowding number ($N = 2/3c_v(L/d)^2$). The crowding number gives the number of fibers that are present in a volume of a sphere with a diameter of the length of the average fiber in the suspension. A crowding number higher than 60 is found in fiber suspensions with continuous fiber contacts.[18] Due to frequent contacts between fibers in suspensions with a crowding number higher than 60 the fibers change the momentum transfer and lower the turbulence level of the flow.[19,20]

The structure of the flow field of pulp suspensions in sudden expansions has recently been studied with positron emission tomography at a concentration of 0.4%.[21] In this study, the degree of disruption in the formed jet after an axisymmetric 1:5 sudden expansion was analyzed when the velocity was varied between 0.5 and 0.9 m/s. At higher velocities a fully disrupted jet was observed. Another study by Yan and Norman[22] focused on floc deformation in the expansion zone in pulp suspensions at a concentration of 0.5% after a 2-D nozzle. Floc deformation was analyzed with a high-speed camera and the findings were used to develop a system for analyzing fiber flocculation. Arola et al.[23] studied the fiber reflocculation time in a circular pipe after an 1:1.7 expansion with nuclear magnetic resonance imaging. Images were taken from both upstream and downstream the expansion zone both in water and in a pulp suspension with a concentration of 0.5% at different velocities. The findings from the experiments on pulp suspension indicate that a higher upstream velocity gives a decrease in plug diameter and an increase in the velocity gradient at the wall in the downstream region due to an unsteady flow of recirculated suspension. The transient fluidization of pulp suspension before and after a contraction in a square channel has also been studied by Karema et al.[24] In their study they focused on floc structure and reflocculation after the contraction unit. Hardwood pulp with a concentration of 1% and softwood pulp with a concentration of 0.5% were studied at different flow rates. Their experimental results show that the size of the flocs scaled by the average velocity in the early stage of reflocculation can be described by a power law.

Turbulence in the mixing layer region of a 2-D water jet has been studied using the ultrasound velocity profiling (UVP) technique with a sampling rate of 30–60 ms by Inoue et al.[25] Flow structures in the mixing layer were analyzed with wavelet transforms and power spectrum. Findings indicate that it is possible to obtain velocity profiles and turbulence characteristics with UVP. The UVP technique has also been shown to give accurate flow measurement in pulp suspensions.[26–28]

The aim of this study was to investigate the flow properties of a 2-D jet of pulp suspension at concentrations above one percent using UVP and a high-speed camera. Pulp jets at concentrations above one percent have, to the authors' knowledge, not been studied in detail before. In the experiments both concentration (1.8 and 2.8 wt % corresponding to crowding numbers of 7,100 and 11,000) and velocity (1-2.2 m/s) were varied. In comparison a crowding number of 60 (the starting point for continuous fiber contacts), corresponding to a concentration of 0.015% only with the fibers used in this study. The data were analyzed for flow field, RMS, dimensions of the jets and the experimental data together with CFD simulations were used in a study of the bulk flow properties in pulp suspension away from the walls.

Pulsed Ultrasound Velocimetry-Ultrasound Velocity Profiling (UVP)

Ultrasound velocity profiling (UVP) is a technique used to measure instantaneous flow profiles along a pulsed beam axis in liquids seeded with particles. The technique was originally developed to measure blood flow, but was later extended to include general fluids.[29] A transducer transmits short emissions of sinusoidal ultrasonic bursts that travel along a measurement axis through the suspension. Directly after the pulses are transmitted, the transducer switches to receiving or "listening" mode. When the ultrasonic pulse hits a small particle in the fluid, parts of the ultrasonic energy scatter on the particles and echo back. The echo reaches the transducer after a time delay. The transmitted pulses are separated by a fixed pulse repetition frequency and the time between the pulses is used for sampling the returning echo. The measurement line is, thus, divided into small measurement volumes or "channels" where data is sampled with different time delays corresponding to different spatial positions along the beam axis.

Part of the ultrasonic energy is reflected on the surface of particles that travel with nonzero velocity components across the measurement axis. The frequency in the received sinusoidal pulse originating from a scattering particle is different from the transmitted frequency and the "doppler-shifted" frequency can be used to calculate the velocity of the measured particle. However, since the relative shift in frequency is much smaller than the emitted frequency, modern instruments do not measure the doppler shift but measure time/phase lags between consecutive pulse emissions instead. Both the time delay between the received pulses as well as the "doppler-shifted" frequency, or more correctly the time/phase lag between pulse emissions are used to determine the position and velocity of particles along the measurement line which gives the instantaneous velocity profile. Velocity estimations are performed both in the time and frequency domain using cross-correlations and fast-Fourier transform (FFT) methods. A complete methodology and system have been developed by Wiklund et al.[30–32]

Experimental Setup

The experimental setup used in this work was based on the flow loop and instrumentation used by Wiklund et al., and Fock et al.,[26,28] but with a modified test section. The flow loop consisted of a 300 L open tank placed on a progressive cavity pump, which gave a maximum flow rate of 180 L/min. A closed stainless steel pipe circulation system with a diameter of 100 mm was connected to the pump. In the downstream region a customized test section was installed in which the jet was studied. The test section and the

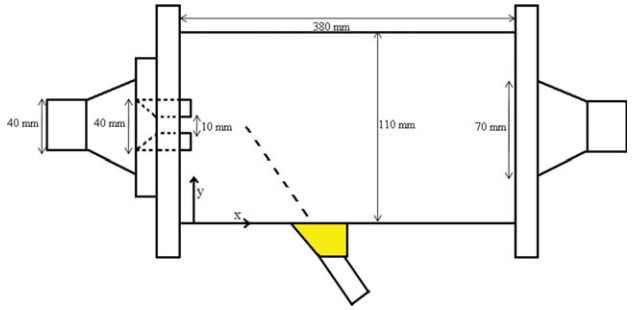

Figure 1. Schematic picture of the test section and the transducer placed in a wedge.

The width of the test section in the *z*-direction is 40 mm. [Color figure can be viewed in the online issue, which is available at wileyonlinelibrary.com.]

stainless steel pipe were connected via a contraction unit that decreased the diameter from 100 mm to 40 mm. The test section was designed as a rectangular conduit (110·380·40 mm) made of 5 mm thick Plexiglas and its dimensions are given in Figure 1. In the test section the pulp suspension flowed through a 1:11 sudden expansion. To minimize the tendency of forming an air pocket in the upper part of the test section a low flow velocity was used in the startup period to slowly fill the test section before the desired velocity was tuned in.

UVP equipment

The UVP system and methodology used in this work is well described in the literature.[30–33] In brief, the setup consisted of a customized UVP-DUO-MX Monitor, from Met-Flow SA, Lausanne, Switzerland. The instrument firmware and driver software were modified to allow access to the complex demodulated baseband signal (I/Q), i.e., raw data. The UVP-Duo instrument and the other hardware devices were connected to a master PC via Ethernet and a high-speed digitizer (DP1400 Acquiris, Agilent Technologies, Kista, Sweden). The digitizer was an integral part of the data acquisition scheme, enabling simultaneous measurements of the flow velocity and acoustic properties. UVP data acquisition was implemented with an Active X library (Met-Flow SA, Lausanne, Switzerland). All data acquisition, data processing and analyses were made using RheoFlow™ software version 3.0, developed at SIK, the Swedish Institute for Food and Biotechnology.

The test section was made of 5 mm thick Plexiglas and comprised a transducer holder, fixed to a linear digital scale (Mitutoyo 572-203-10, Mitutoyo Scandinavia AB, Upplands Väsby, SWEDEN) that enabled traversing the transducers, with a spatial resolution of 0.04 mm, in the x-direction at the center under the test section. All flow profiles were, thus, measured with a single transducer placed at the center under the test section at different spatial positions, see Figure 1. A custom made 4 MHz transducer (TR0405LH-X, Signal-Processing SA, Switzerland) was used in combination with an acoustic wedge (ABWM, Olympus Sverige AB, Solna, Sweden). The wedge angle was 45° between the top of the transducer and the Plexiglas wall for producing a well-defined ultrasonic pulse path from and back to the transducer for the transmitted and received pulses. The setup used resulted in a refractive angle of 18.7° in the suspension due to the index of refraction in the Plexiglas and the pulp suspension. Experimental UVP measurement parameters are given in Table 1.

Table 1. Experimental UVP Parameters

Ultrasound frequency	4 MHz
Number of cycles per pulse	4
Burst per profile/pulse repetitions per profile	512 and 860
Measurement time	60 seconds
Time resolution (single profile)	110-581 ms/profile
Sampling rate	9.1-1.7Hz
Number of recorded profiles per flow rate	103-545
Sound velocity in suspensions	1485-1490 m/s
Doppler angle in suspensions	18.7°
Channel width	0.74mm
Channel distance	0.37mm
Velocity resolution	1.3-16.7 mm/s
Number of recorded channels	212-300

In order to be able to study the frequency in the boundary layer the measurement time was set at 60 s. The measurement time was a compromise between the total experimental time and the low-data rate. According to Table 1, the time resolution varied with measurement conditions. The time resolution increased along the jet due to the decrease in flow rate since a lower pulse repetition frequency (PRF) had to be used in order to achieve the same measurement accuracy for lower flow rates. As a result of the decision to perform all measurements over a period of 60 s, the number of profiles varied with time resolution. In almost all measurements the number of recorded channels was 300, but for the jets with a 2.8% pulp suspension, the number of channels was decreased for the positions until $x = 50\%$.

Material and experimental procedure

Fully bleached never-dried kraft pulp provided by Södra Cell Värö was used in the experiments. The pulp was collected from the end of the last bleaching step, and it had an initial concentration of around 20% fibers. The mean length of the fibers was 2.0 mm, and the mean diameter was 26 μm. In the experiments, pulp suspensions at 1.8 and 2.8 wt % were investigated. Three jets were studied at each concentration. Before the experiments were performed the pulp was diluted from 20% to the desired concentration, and the mixture was stirred to disrupt larger floc structures. At each concentration approximately 140 L pulp suspensions were used. First, all measurements for the three jets at the pulp concentration of 1.8% were made. The flow loop was then emptied and filled with new, fresh 2.8% pulp suspension. In Table 2 the jet lengths, the average velocities U_0, of the jets at $x = 0$, and measurement positions studied are summarized for each concentration.

Both visual observations with a Fastcam PCI, Model 2 K high-speed camera, made by Photron, and velocity measurements with the UVP were used in a pre-study to find reasonable measurement parameters. In the pre-study the correlation between the velocity and the jet length in pulp

Table 2. Jet Properties and Measurement Positions

Concentration (%)	Length (mm)	U_0 (m/s)	Measurement position in the x direction (% of total jet length)
1.8	50	1	25, 50, 75, 100
2.8	50	1.5	25, 50, 75, 100
1.8	80	1.2	12.5, 25, 37.5, 50, 62.5, 75, 87.5, 100
2.8	80	1.8	12.5, 25, 37.5, 50, 62.5, 75, 87.5, 100
1.8	100	1.5	33 37.5, 50, 62.5, 87.5, 100
2.8	100	2.2	33 37.5, 50, 62.5, 87.5, 100

suspensions with a concentration of 1.8 and 2.8% was studied. The final measurement parameters were determined from these experiments. The length of the jets studied correspond to the distance from $x = 0$, according to Figure 1, to the position where the velocity measured in the center of the jet was 6.5 ± 0.2 times higher than the velocity measured in the fully developed region further downstream. The velocities at U_0 that gave a jet length of 100, 80 and 50 mm were chosen.

Rheology

The rheology of fiber-water suspensions has been studied for some years, but details are still unknown.[7] Both flow and fluid properties change when the flow rate changes. Fiber orientation is dependent on flow conditions and network strength. Differences in the packing of fibers in the network, due to fiber dimensions and flocculation, create irregularities in the network. Dewatering effects occur near solid surfaces. These factors complicate the derivation of a valid rheology model.[6]

When the flow properties of pulp suspensions have been studied, experiments have shown that a certain critical stress, a yield stress, needs to be exceeded before pulp suspensions start to move. In the laminar regime, fibers are locked in the network. When the flow rate is increased, the fiber network starts to disrupt and, in the turbulent regime, the network is totally disrupted and the fibers are mobile. The flow behavior in the laminar regime has similarities with a non-Newtonian single-phase fluid, and a turbulent pulp suspension has similarities with a Newtonian turbulent flow.[34,35] One of the simplest rheology models describing single-phase non-Newtonian fluids in the laminar flow regime including a yield stress is the Bingham plastic model, which is a limiting case (with n equal to 1) of the general Herschel-Bulkley equation

$$\tau_{x,y} = \tau_y + K\left(\frac{\partial U_x}{\partial y}\right)^n \quad (1)$$

The first part, on the righthand side in Eq. 1 corresponds to the yield stress, and the second to the flow properties after yielding. Yield stress is defined as the force needed to create movement in a static fluid. Furthermore, the constant K is related to the viscosity at infinite shear, and the exponent n is related to shearing effects after yielding.

In contrast to single-phase non-Newtonian fluids as mentioned previously, pulp suspensions in the laminar flow regime have a varying apparent viscosity and local network strength due to local fiber orientation, therefore, no exact figures on these parameters are possible to determine. However, studies in pipe flows of pulp suspensions using the Herchel-Bulkey model in the laminar regime with a viscosity of water after yielding, an exponent n equal to 1 and an experimentally measured yield stress, have been shown to capture the main flow effects at low shear rates.[1,36–38] However, there are indications of shear thinning effects in pulp suspensions that cannot be captured with a decreasing n.[1]

To investigate fiber network properties, fiber dimensions as well as yield stress were measured in the two suspensions. Samples from the suspensions were measured before the experiments were started, halfway through and after the measurement sequence was finished. These measurements were made in order to investigate if the pump changed the network properties. The yield stress was measured with a Viscolab LC1 rheometer made by Physica. More details about the rheometer are given in Andersson et al.[39] The fiber dimensions were measured with a Kajaani FS300 made by Metso. The measurements showed that the changes in fiber dimensions and yield stress were negligible over the measurement time. The average measured yield stress was 145 Pa for the 1.8% concentration and 245 Pa for the 2.8% suspension. Furthermore, no experiments measuring the viscosity were made due to a lack of reliable measurement techniques in fiber suspensions.[9] However, the apparent viscosity of pulp suspensions in fully disrupted fluids where the fibers are free to follow the flow may be estimated from a correlation by Bennington and Kerekes.[40] This correlation gives an apparent viscosity of 0.009 Pas for the suspension with a concentration of 1.8%, and 0.036 Pas for the suspension with a concentration of 2.8%.

Numerical Simulations

To investigate if the Bingham plastic model is valid for the studied suspensions, numerical simulations were performed using the computational fluid dynamic (CFD) program ANSYS CFX-13.0. In the simulation, the Navier-Stokes equation and the continuity equation were solved over a defined mesh. In this study, a mesh with 10,746 nodes and 9005 elements was constructed in 2-D geometry with the same size as the real measurement volume. The mesh was a tetrahedrical mesh with denser packing in the contraction part as well as close to the walls. The boundary conditions used were the measured average velocity at the inlet, no-slip at the walls, and average pressure at the outlet and symmetry at the surfaces of the 2-D geometry. When no-slip is used as the boundary condition at the walls, the pressure drop will be overestimated but its influence on the flow structures far away from the walls has been shown to be limited.[41] The rheology of the pulp suspensions is included with the standard non-Newtonian Herchel-Bulkey model available in the software. The exponent n, was set to 1 and the effective viscosity using a limiting viscosity of water was used in regions where the yield stress was exceeded.[1,36–38] It was found that simulations using the measured yield stress values gave too short jets. Thus, the values were subsequently reduced to match the experimental jet lengths.

Results

The flow structures of the jets were studied in the images captured with the high-speed camera. An image from the jet with a concentration of 1.8%, and an average inlet velocity of 1.5 m/s at $x = 0$ is shown in Figure 2 (500 images/s). The picture was taken perpendicular to the flow, directly after the

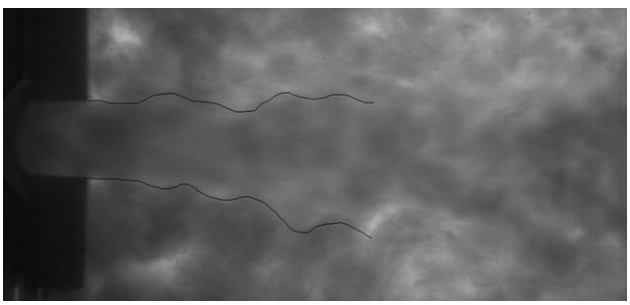

Figure 2. High-speed camera picture of the jet at a concentration of 1.8% and an average inlet velocity of 1.5 m/s at $x = 0$.

The border is highlighted to increase the visibility of the jet.

contraction shown in Figure 1. The general flow structure observed has similarities with a jet that flows toward a wall. Jets of different lengths were formed depending on energy content and network strength. From the images it can be seen that flocs in the recirculation zone below and above the jet were deformed and attached to the jet boundary. The boundary oscillated at a rather fixed frequency. These trends were similar for all jets, but for the faster jets the oscillations at the boundary were more pronounced. From the measurements with UVP, the frequency in the mixing layers was investigated, but no significant frequency could be found since the sampling rate was too low and the data fluctuated with time.

UVP Measurements

General trends

The average velocity and root mean square (RMS) profiles were studied for all measurement positions. The RMS values were calculated by Eq. 2, where u_i are the measured velocities, U_{avg} is the averaged velocity, and M is the number of measurements performed

$$u' = \sqrt{\frac{\sum_{i=1}^{M} \left(u_i - U_{avg}\right)^2}{M}} \tag{2}$$

The general trends for the profiles measured at the same percent of the total length were similar for all jets studied. At longer distances from the entrance, there were some tendencies for the jet to change direction. To compensate for this, the profiles after a jet length of 60% were moved a few millimeters upward in the y direction in all figures presented. To illustrate typical profiles, the case at a concentration of 1.8%, and an average inlet velocity of 1.2 m/s at $x = 0$ is shown in Figure 3. The average velocity measured at each position is scaled with the average velocity at the inlet (see Table 2). Also included in the figure are lines marking the position where the measurements were made (given in Table 2). The velocity and the RMS profiles were scaled with U_0. All u'/U_0 values are scaled by 0.5 to avoid the overlap between the RMS profiles.

In Figure 3, the velocity profiles show that the diameter increases and the velocity decrease along the jet. Furthermore, a recirculation zone was also observed in the average velocity profiles. According to Figure 3 (top), the recirculation zone is found in measurements performed closest to the orifice until 62.5% of the total jet length. The RMS plot describes the mean velocity fluctuations at each point. When

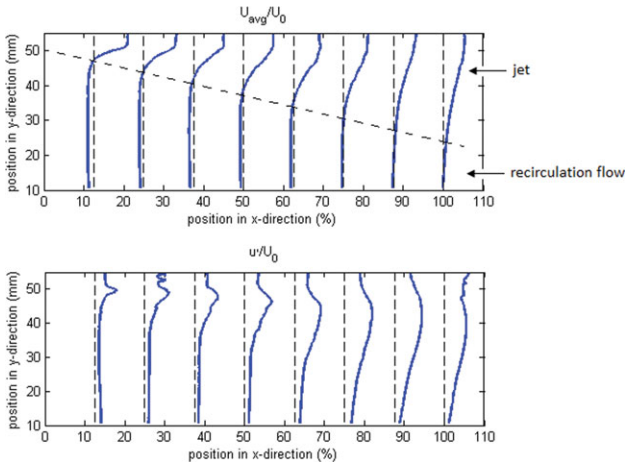

Figure 3. Scaled average velocity profiles (top), and RMS velocities (bottom) along the jet at a concentration of 1.8%, and an average velocity of 1.2 m/s at $x = 0$.

In the figure $y = 0$ is located at the lower wall. [Color figure can be viewed in the online issue, which is available at wileyonlinelibrary.com.]

examining the RMS profiles, it can be seen that the profiles peak in the mixing layer between the jet and the surrounding fluid. According to the RMS plot shown in Figure 3, the width of the mixing layer was found to increase along the jet. This indicates that the size of the region in which the bulk flow and the jet flow interact increased with increasing jet length. The core of the jet above the mixing layer closest to the center of the geometry appeared to be more or less constant along the jet and the main increase in width was caused by an increase in the size of the mixing layer. These behaviors have also been discussed by Heat et al. and Arola et al.[21,23]

Comparison of the Jets

To study the impact of changes in velocity and concentration, the experimental results from the six cases presented in Table 2 were compared.

Scaled velocity profiles

The average flow profiles along the six studied jets are plotted in Figure 4. All profiles were scaled with U_0 for each specific case. According to Figure 4, all jets studied show similar profiles along the jet independent of velocity or concentration.

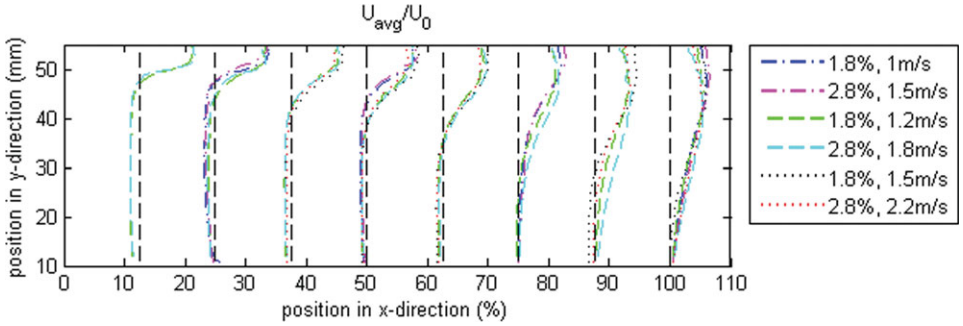

Figure 4. The scaled average velocity profiles along all studied jets. In the figure $y = 0$ is located at the lower wall.

[Color figure can be viewed in the online issue, which is available at wileyonlinelibrary.com.]

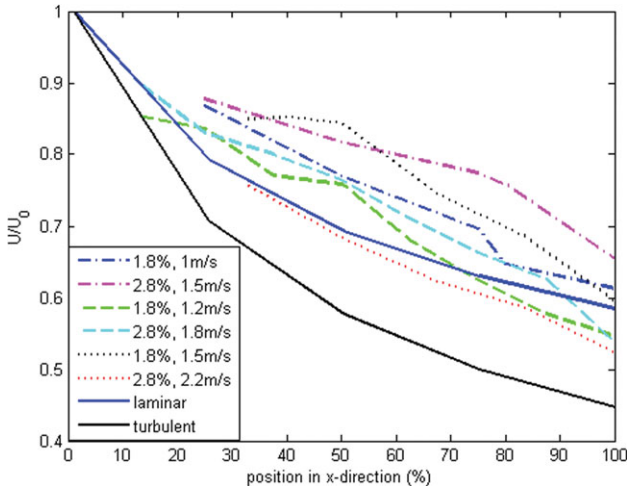

Figure 5. The decrease in centerline velocity for all studied jets as well as the theoretical laminar and turbulent free jets.

[Color figure can be viewed in the online issue, which is available at wileyonlinelibrary.com.]

Centerline velocity along the jet

Figure 5 shows, the decrease in centerline velocities for all studied pulp jets and the theoretical values for free planar Newtonian laminar and turbulent jets. The decrease in the centerline velocity for a free planar Newtonian laminar jet is theoretically proportional to $x^{-1/3}$, and for a turbulent jet to $x^{-1/2}$.[42]

According to Figure 5, the decrease in centerline velocity for the studied pulp jets is approximately linear. Furthermore, the results from the comparison of the pulp jets at the same concentration show a faster decrease in the centerline velocity for jets with a higher inlet velocity. This was observed for all jets except the jet with a concentration of 1.8% and an inlet velocity of 1.5 m/s. When jets with the same length were compared it was observed that the centerline velocity decreased faster at a lower concentration for the jets with a length of 50 mm and 80 mm in contrast to jets with a length of 100 mm. Deviations were seen, as expected, when comparing the experimental centerline velocity profiles with the theoretical Newtonian jets.

RMS velocity along the jet

The measured RMS profiles along the x-direction are plotted in Figure 6 for all jets. All profiles are scaled with U_0 and, to avoid the overlap between the RMS profiles, all u'/U_0 values are scaled by 0.5. Also the profile at 25% of the total jet length for the jet with a concentration of 2.8%, and an average inlet velocity of 1 m/s at $x = 0$ is not included due to high-noise peaks that affect the visibility of the other profiles. Disregarding the noise peaks, however, the size of the RMS peak in this profile follow the trend of the other jets. The half width of the jet is defined as the distance from the center of the jet to the position with the highest RMS value, marked with the black line in Figure 6. From the results it was seen that the width increased along the jet. The mixing layer that describes the region between the jet core and the surrounding suspension was estimated to be the width of the RMS peak. In Figure 6, the mixing layer is marked with blue lines and it increases along the jet.

In Figures 7a and b, the increases in the width of the mixing layer along the x-axis, as well as the maximum RMS velocity along the expansion length, are presented. It can be seen that an increase in velocity gave a wider mixing layer in the downstream region. Furthermore, at the same measured jet length, a higher concentration gave a wider peak. When the height of the peak was studied, see Figure 7b, it was observed to increase with concentration for all cases except the one with a concentration of 1.8%, and an average velocity of 1.5 m/s for jets with the same jet length. However, no changes in RMS values, in the two experiments performed at an average velocity of 1.5 m/s, were observed. An increase in RMS with increased concentration was also observed in particulate flows.[12]

Width of the jet

When the jet width was studied, only the lower half of the jet was analyzed due to noise in the UVP signal in the upper part of the jet, which was induced by fluctuations in velocity. As stated earlier, the half width of the jet was estimated to be the length from the center of the jet to the position with the highest RMS velocity marked in Figure 6. However, in both Figure 8a and 8b the core region was excluded to increase visibility. To get the real jet width measured, 5 mm should be added to all data. In Figure 8a, the estimated half widths of the jets scaled with the percent of the total jet length are compared with the theoretical values for the spreading of a free laminar planar Newtonian jet (proportional to $x^{2/3}$).[42] The spreading rate of the theoretical laminar jet and the pulp jets at the actual position in the x-direction are shown in Figure 8b. The width of a free Newtonian turbulent jet increased much faster (proportional to x)[42], and is excluded from Figures 8a and b.

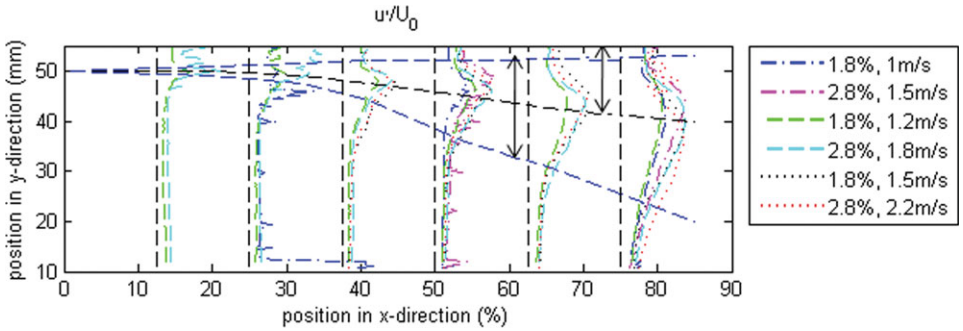

Figure 6. The scaled RMS velocity along all studied jets.

The black line shows the half width of the jet and the two blue lines show the width of the mixing layer. In the figure $y = 0$ is located at the lower wall. [Color figure can be viewed in the online issue, which is available at wileyonlinelibrary.com.]

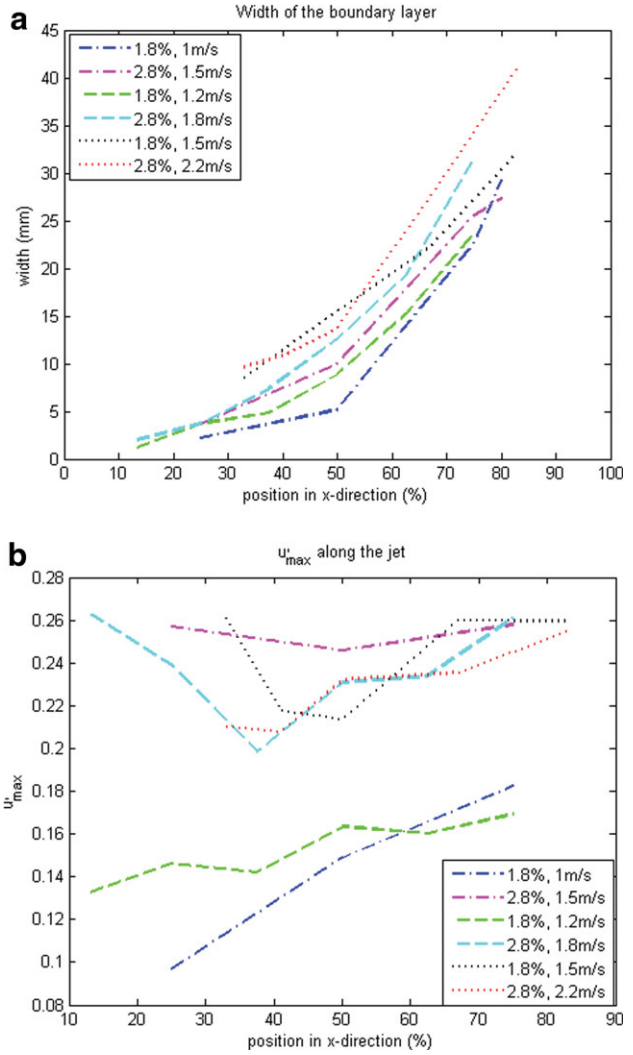

Figure 7. (a) The increase in width of the mixing layer along the six studied jets; (b) the maximum RMS velocity along the six studied jets.

[Color figure can be viewed in the online issue, which is available at wileyonlinelibrary.com.]

According to Figure 8a the increase in width for the studied pulp jets could be described by a linear equation with an intercept at 5 mm, a slope of 0.09 at the two higher velocities, and 0.055 at the lower velocity independent of concentration. The faster increase in width at the higher inflow velocities was not as clear when the width of the mixing layer was investigated, which also gives an indication of the jet increase. This indicates that the position of the peak is closer to the jet core in pulp jets with a lower velocity. The influence of concentration appeared to have a minor impact on the width when it was related to the position of the peak. When the pulp jets in Figure 8b are compared it can be seen that a jet with a higher velocity is thinner at the same axial position. According to Figure 8a the theoretical laminar Newtonian jet is wider than the pulp jets and from Figure 8b it can be concluded that the spreading angle is wider for a theoretical Newtonian laminar jet.

Discussion of Experimental Results

From the experiments it was found that the centerline velocity decreased faster and the jet width increased more for jets with a higher inflow velocity. When the concentration was increased and the jet length was kept constant the decrease in centerline velocity was slower, and the width seems to be unaffected according to Figure 5. However, a faster increase of the mixing layer with increasing concentration was observed (Figure 7a). The decrease in centerline velocity and increase in jet width is established when the jet captures parts of the slower moving surrounding fluid. A faster jet has a larger surface area, which implies that the friction forces between the jet border and the surrounding suspension are greater, which results in a faster decrease in centerline velocity and an increase in width. The friction forces in the mixing layer will also increase when the concentration is increased, which results in a faster increase in width. However, the centerline velocity was more stable at a higher concentration probably due to the higher network strength in the core region of the jet, which implies that it was more difficult to disrupt.

When Figures 5 and 8 are studied it can be seen that the decrease in centerline velocity and the increase in width is faster in a Newtonian jet than in the studied pulp jets. These properties have also been observed in particulate flows.[10,11] As mentioned earlier, fiber suspensions in the turbulent flow

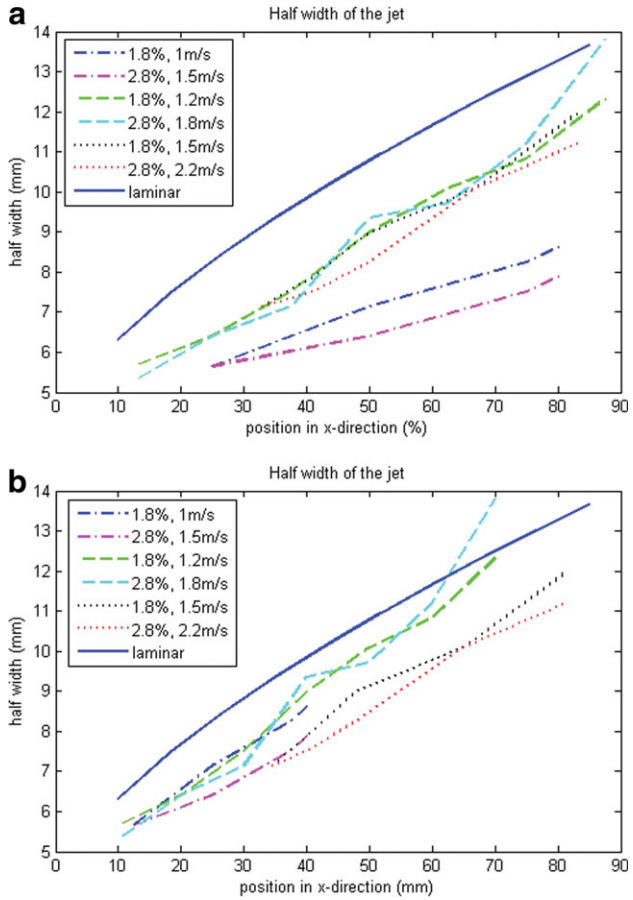

Figure 8. (a) The width of the six pulp jets as well as the Newtonian laminar free jet scaled with the percental length of the total jet length; (b) visualization of the spreading rate of the six studied pulp jets and the Newtonian laminar free jet.

[Color figure can be viewed in the online issue, which is available at wileyonlinelibrary.com.]

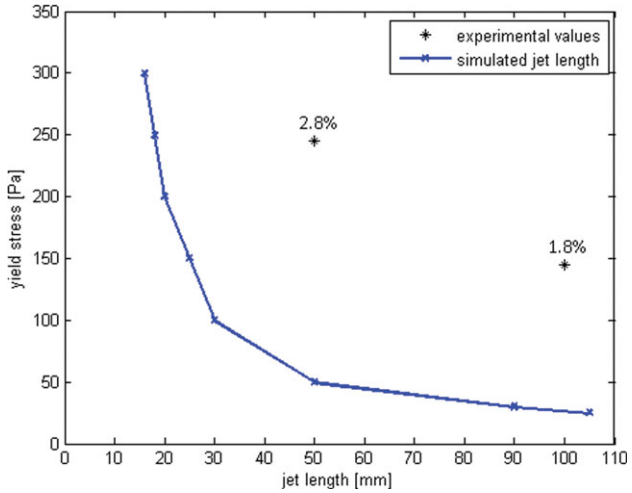

Figure 9. The simulated jet length compared to the measured jet length in the experiments at an average velocity of 1.5 m/s at $x = 0$.

[Color figure can be viewed in the online issue, which is available at wileyonlinelibrary.com.]

regime show similarities with Newtonian flows. This implies that turbulent pulp jets can be described by the equations valid for theoretical turbulent Newtonian jets. However, this was not seen in Figure 5 or 8 which implies that the studied pulp jets are probably not in the turbulent flow regime. In the laminar flow regime pulp suspensions are non-Newtonian and fluid properties, such as apparent viscosity, changes along the jet. This implies that the theoretical Newtonian laminar flow model cannot capture the flow properties of pulp suspensions in this regime. Furthermore, the change in fluid properties due to changes in concentration or velocity also implies that no similarity solution is valid in the laminar flow regime as also found in non-Newtonian fluids.[14]

Comparisons with the theoretical Newtonian jets indicated that the jets studied were not turbulent. However, the similarity between a Newtonian turbulent jet and pulp jets at the consistencies studied has never been investigated earlier, and, therefore, the conclusion regarding turbulence is difficult to determine without having experimental data at a higher sampling rate. An estimate of the frequency needed to capture the turbulence structures in the mixing layer at a velocity of 1.5 m/s for the smallest eddies assumed to be about the size of the fiber length (2 mm) gives a frequency of 750 Hz. The largest eddies should be in the size of the mixing layer, which gives a frequency of approximately 100

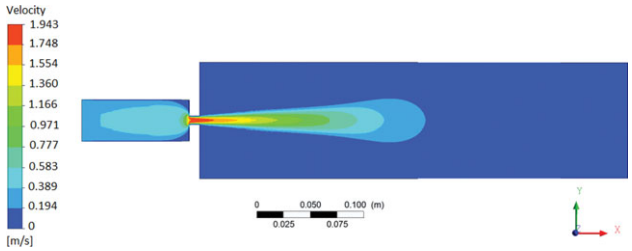

Figure 10. The magnitude of the velocity of a jet with a yield stress of 25 Pa at an inflow velocity of 1.5 m/s captured in the CFD simulations.

[Color figure can be viewed in the online issue, which is available at wileyonlinelibrary.com.]

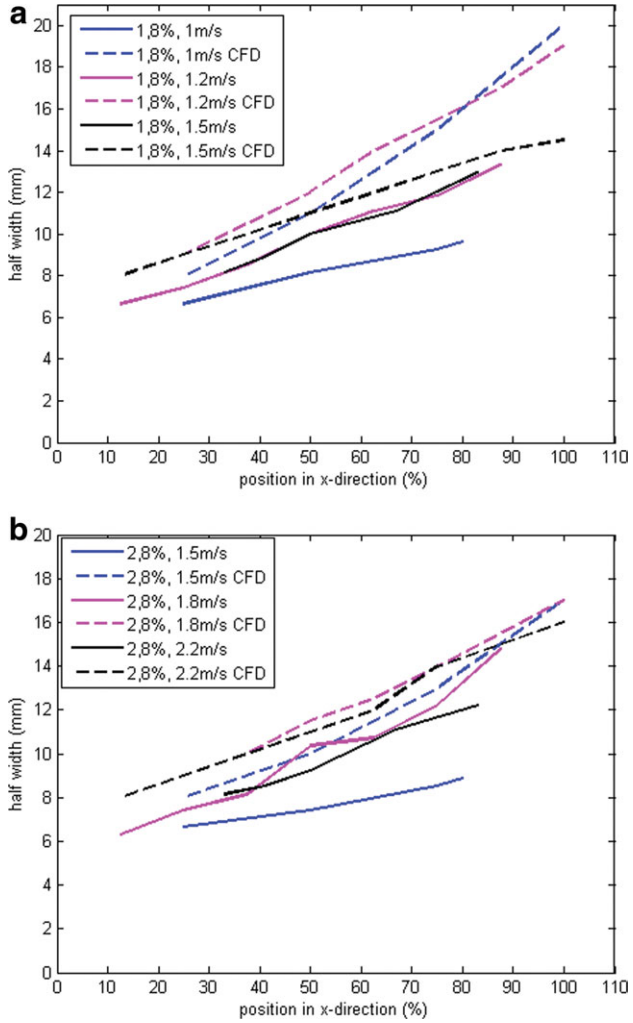

Figure 11. (a) Comparison between the measured half width of the jet (Figure 8a) with the simulated half width of the jet using a yield stress of 25 Pa instead of the measured at 145 Pa; (b) comparison between the measured half width of the jet (Figure 8a) with the simulated half width of the jet using a yield stress of 50 Pa instead of the measured at 245 Pa.

[Color figure can be viewed in the online issue, which is available at wileyonlinelibrary.com.]

Hz. The sampling rate used in the experiments presented in Table 1 was a factor 100 lower than the estimated frequency. However, analyses of the images taken with the high-speed camera show an undisrupted jet core which indicates that the flow was in the laminar regime. This implies that the estimated viscosities mentioned earlier are invalid, and, therefore, no estimated Reynolds number can be calculated.

Non-Newtonian Rheology Model

To investigate if the laminar single-phase non-Newtonian Bingham plastic rheology model could capture the flow structure in the studied pulp jets, calculations with CFD were performed. In the comparison, simulations of the two studied pulp jets, with an average velocity U_0, equal to 1.5 m/s, were made. The Herchel-Bulkely model was used as the non-Newtonian viscosity model with K equal to 0.001

Pas, n equal to 1 and τ_y equal to 145 Pa and 245 Pa. In accordance with the jet length measured in the experiments, the part of the jet studied in the simulations corresponded to the distance from $x = 0$, according to Figure 1, to the position where the velocity measured in the center of the jet was 6.5 times higher than the velocity measured in the fully developed region further downstream. From the findings it was seen that the main difference between the simulated non-Newtonian jets and the studied pulp jets was the resulting jet length, where the simulated jets were 2.8–5.2 times shorter. To investigate the impact from yield stress and the shear thinning effects on the jet length (see Eq. 1) simulations with decreasing τ_y and n were made. From those simulations it was concluded that a decrease in n from 1 to 0.1 did not change the jet length. However, as expected, a decrease in yield stress increased jet length. Results from the simulations with a decrease in yield stress are shown in Figure 9.

According to Figure 9, a yield stress of approximately 25 Pa captured the length of the pulp jet with a concentration of 1.8%, and a yield stress of approximately 50 Pa captured the length of the pulp jet with a concentration of 2.8%. From these findings it was concluded that the measured yield stress has to be decreased by approximately 80% to capture the measured length of the studied pulp jets. Consequently, the Bingham plastic model cannot capture the flow properties of the pulp jets if the measured yield stress from a rheometer is used. In a rheometer, the yield stress measured is the force needed to create movement in a static fluid. However, when a pulp jet is studied, the retardation of the jet is mainly established in the mixing layer where the jet border is slowed down by the recirculated fluid outside the jet. Furthermore, in the mixing layer the network is broken, which results in a lower transport of momentum from the surrounding suspension to the jet in comparison to the momentum transport in an unbroken network. This implies that the yield stress in the mixing layer is lower than the yield stress measured in a rheometer. Figure 10 shows the magnitude of the velocity from the simulation of the jet with an inflow velocity of 1.5 m/s and a yield stress of 25 Pa. Similar images of the velocity profile were found in all the simulations. According to Figure 10, the centerline velocity decreases and the width increases along the jet, in accordance with the experimental result as depicted in Figure 2.

To further investigate if the measured jet dimensions could be captured with the standard Bingham plastic model using the yield stresses in Figure 9, simulations with a yield stress of 25 and 50 Pa were performed. The only parameter changed, besides yield stress, was the inlet condition where the average inflow velocities given in Table 2 were used. The results from the simulations show that the length of the simulated jet deviated approximately $\pm 10\%$ from the experimental ones. At the lower concentration, the jet length was underestimated at the lower inflow velocities, and at the higher concentration the jet length was overestimated for the higher velocities. The difference was the greatest at the lower concentration. According to these results, yield stress increases with an increase in velocity. To further investigate the similarities between the measured and simulated jets, the increase in jet width was compared, and the results are presented in Figure 11. Figure 11a shows the jet width at the lower concentration, and Figure 11b shows the jet width at the higher concentration.

According to Figure 11, the simulated half width of the jets was slightly higher with the largest deviations at the lower concentration (Figure 11a). It can be concluded that the non-Newtonian Bingham plastic model captured the main flow structures using an estimated yield stress. Furthermore, the deviations in the jet dimensions, especially the final jet length, between the simulated and measured jets at different flow rates indicate that the velocity has an impact on the yield stress.

Conclusions

In this study, six pulp jets at consistencies of 1.8 and 2.8% were studied at different flow rates using UVP. The UVP technique was successfully used to obtain instantaneous velocity profiles and RMS values in flows of the concentrated fiber suspensions after a sudden expansion.

The scaled velocity profiles of the jets were compared and the velocity fluctuations in the mixing layer were investigated. Conclusions from the results from measurements at the same percent of the total jet length conducted without changing the concentration, show that the scaled centerline velocity decreased faster, and the width of the jet increased more when the flow rate was increased. The decrease in the centerline velocity and the increase in the width of a jet are mainly established in the mixing layer. A faster jet has a larger surface between the jet core and the surrounding suspension, which implies that the frictions forces are greater which results in a faster decrease in velocity and increase in width. The effects of an increase in concentration were observed to give a slower decrease in centerline velocity and a faster increase in the width of the mixing layer for jets with the same jet length (see Figure 7a). At a higher concentration, the network strength was higher which implies that the core region in the jet was more difficult to disrupt and the centerline velocity was more stable. However, the higher network strength results in higher friction forces in the mixing layer, a larger part of the fiber network in the surrounding suspension is affected by the jet, and the width of the jet increases faster.

CFD simulations including the standard Bingham plastic non-Newtonian viscous model were performed for all studied pulp jets. Comparison with the measured jet dimension show that it was possible to capture the main flow properties in the simulations if the measured yield stress was decreased by approximately 80%. This implies that the shear decreases the network strength in the flow domain. The network strength in the shear field may be regarded as an apparent yield stress. To further investigate the rheology of pulp suspensions, an experimental technique with the potential of measuring the network strength in the flow domain is required. The experimental information from this study would make valuable input for this task.

Acknowledgments

This work is part of a PhD project financed by the Swedish Energy Agency. Emma Levenstam Bragd from SIK is gratefully acknowledged for her experimental assistance.

Notation

C_v = volume concentration, %
D = jet orifice diameter, m
d = diameter of a fiber, m
K = concentration coefficient in non-Newtonian model, Pas
L = length of a fiber, m

M = number of measurements
n = power index for a non-Newtonian fluid
N = crowding number
U = velocity, m/s
U_0 = bulk velocity at the orifice, m/s
U_{avg} = average velocity, m/s
u' = RMS velocity, m/s
x = coordinate in the flow direction
Y = yield number
y = coordinate perpendicular to the flow direction
μ_{ref} = reference viscosity, Pas
τ_y = yield stress, Pa

Literature

1. Wikström T, Rasmuson A. The agitation of pulp suspensions with a jet nozzle agitator. *Nordic Pulp Paper Res J*. 1998;13:88–94.
2. Feng H, Olsen MG, Liu Y, Fox RO, Hill JC. Investigation of turbulent mixing in a confined planar-jet reactor. *AIChE J*. 2005;51: 2649–2664.
3. Jordan C, Rankin GW, Sridhar K. A study of submerged pseudoplastic laminar jets. *J Non-Newtonian Fluid Mech*. 1992;41: 323–337.
4. Schlichting DH. *Boundary-Layer Theory*. New York, NY: McGraw-Hill, Inc; 1968.
5. Rajaratnam N. *Turbulent Jets*. New York: Elsevier Scientific Publishing Co; 1976.
6. Fock H, Claesson J, Wikstrom T, Rasmuson A. Near wall effects in the plug flow of pulp suspensions. *Can J Chem Eng*. 2011;89: 1207–1216.
7. Duffy GG. The significance of mechanistic-based models in fibre suspension flow. *Nordic Pulp Paper Res J*. 2003;18:74–80.
8. Paul EL, Atiemo-Obeng VA, Kresta SM, eds. *Handbook of Industrial Mixing*. Hoboken, NJ: John Wiley & Sons, Inc; 2004.
9. Derakhshandeh B, Kerekes RJ, Hatzikiriakos SG, Bennington CPJ. Rheology of pulp fibre suspensions: A critical review. *Chem Eng Sci*. 2011;66:3460–347.
10. Fan J, Zhao H, Can K. An experimental-study of 2-phase turbulent coaxial jets. *Experiments Fluids*. 1992;13:279–287.
11. Sheen HJ, Jou BH, Lee YT. Effect of particle-size on a 2-phase turbulent jet. *Exp Therm Fluid Sci*. 1994;8:315–327.
12. Virdung T, Rasmuson A. Hydrodynamic properties of a turbulent confined solid-liquid jet evaluated using PIV and CFD. *Chem Eng Sci*. 2007;62:5963–5978.
13. Jafri IH, Vradis GC. The evolution of laminar jets of Herschel-Bulkley fluids. *Int J Heat Mass Transfer*. 1997;41:3575–3588.
14. Stehr H, Schneider W. Jet flows in non-Newtonian fluids. *ZAMP*. 2000;51:922–941.
15. Lundell F, Söderberg D, Alfredsson H. Fluid mechanics of papermaking. *Ann Rev Fluid Mech*. 2011;43:195–217.
16. Fock H, Rasmuson A. Near wall studies of pulp suspension flow using PIV. *Nordic Pulp Paper Res J*. 2008;23:120–125.
17. Pettersson AJ, Wikström T, Rasmuson A. Near wall studies of pulp suspension flow using LDA. *Can J Chem Eng*. 2006;84:422–430.
18. Kerekes RJ, Soszynski RM, Doo PAT. *The flocculation of pulp fibers*. In: *Eighth Fundamental Research Symposium*. Oxford, UK: Mechanical Engineering Publishing, Ltd; 1985:65–310.
19. Steen M. On turbulence structure in vertical pipe flow of fiber suspensions. *Nordic Pulp Paper Res J*. 1989;4:244–252.
20. Kerekes R J. Rheology of fibre suspensions in papermaking: An overview of recent research. *Nordic Pulp Paper Res J*. 2006;21: 598–612.
21. Heath SJ, Olson JA, Buckley KR, Lapi S Ruth TJ, Martinez DM. Visualization of the flow of a fiber suspension through a sudden expansion using PET. *AIChE J*. 2007;53:327–334.
22. Yan H, Norman B. A flow loop system for study of fiber suspension flocculation. *Nordic Pulp Paper Res J*. 2006;21:19–24.
23. Arola DF, Powell RL, McCarthy MJ, Li T-Q, Ödberg L. NMR imaging of pulp suspensions flowing through an abrupt pipe expansion. *AIChE J*. 1998;44:2597–2606.
24. Karema H, Kataja M, Kellomäki M, Salmela J, Selenius P. Transient fluidization of fibre suspension in straight channel flow. TAPPI International Paper Physics Conference; 1999:369–379.
25. Inoue Y, Yamashita S, Kondo K. The ultrasonic velocity profile measurements of flow structure in the near field of a square free jet. *Experiments Fluids*. 2002;32:170–178.
26. Wiklund JA, Stading M, Pettersson AJ, Rasmuson A. A comparative study of UVP and LDA techniques for pulp suspensions in pipe flow. *AIChE J*. 2006;52:484–495.
27. Ein-Mozaffari F, Bennington CPJ, Dumount GA, Buckingham D. Measuring flow velocity in pulp suspension mixing using ultrasonic doppler velocimetry. *Chem Eng Res Des*. 2007;85:591–597.
28. Fock H, Wiklund J, Rasmuson A. Ultrasound velocity profile (UVP) measurements of pulp suspensions flow near the wall. *J Pulp Paper Sci*. 2009;35:26–33.
29. Takeda Y. Development of an ultrasound velocity profile monitor. *Nuclear Eng Des*. 1991;126:277–284.
30. Wiklund J, Johansson M, Shaik J, Fischer P, Windhab E, Stading M, Hermansson AM. *In-line Ultrasound based Rheometry of industrial and model suspensions flowing through pipes*. In: *Third International Symposium on Ultrasonic Doppler Methods for Fluid Mechanics and Fluid Engineering*. Lausanne, Switzerland; 2002:69–76.
31. Wiklund J. Ultasound Doppler Based In-Line Rheometry - Development, Validation and Application [PhD Thesis]. Lund University, Sweden; 2007.
32. Wiklund J, Shahram I, Stading M. Methodology for in-line rheology by ultrasound Doppler velocity profiling and pressure difference techniques. *Chem Eng Sci*. 2007;62:4277–4239.
33. Wiklund J, Stading, M. Application of in-line ultrasound Doppler-based UVP-PD rheometry method to concentrated model and industrial suspensions. *Flow Meas Instrum*. 2008;19:171–179.
34. Gullichsen J, Härkönen E. Medium consistency technology, I, fundamental data. *Tappi J*. 1981;63:66–72.
35. Bennington CPJ, Kerekes RJ, Grace JR. The yield stress of fiber suspensions. *Can J Chem Eng*. 1990;68:823–828.
36. Fock H, Wikstrom T, Rasmuson A. CFD modeling of non-Newtonian fluid mixing accounting for transient changes in local solids concentration - application to an agitated pulp stock chest. *Nordic Pulp Paper Res J*. 2010;25:56–64.
37. Ford C, Ein-Mozaffari F, Bennington CPJ, Taghipour F. Simulation of mixing dynamics in agitated pulp stock chest using CFD. *AIChE J*. 2006;52:3562–3569.
38. Gullichsen J, and Härkönen E. Medium consistency technology part 1, fundamental data. *Tappi J*. 1974;64:69–72.
39. Andersson SR, Ringner J, Rasmuson A. The network strength of non-flocculated fibre suspensions. *Nordic Pulp Paper Res J*. 1999;14:61–70.
40. Bennington CPJ, Kerekes RJ. Power requirements for pulp suspension fluidization. *Tappi J*. 1996;2:253–258.
41. Wikström T, Rasmuson A. Transition modelling of pulp suspensions applied to a pressure screen. *J Pulp Paper Sci*. 2002;28:374–378.
42. Bird RB, Stewart WE, Lightfoot EN. *Transport Phenomena*. 2nd ed. Hoboken, NJ: John Wiley & Sons, Inc., 2007.

Manuscript received Mar. 5, 2012, and revision received Jun. 19, 2012.